The Journal of Experimental Biology 208, 3835-3849
Published by The Company of Biologists 2005
doi:10.1242/jeb.01856

Submerged swimming of the great cormorant *Phalacrocorax carbo sinensis* is a variant of the burst-and-glide gait

Gal Ribak[1], Daniel Weihs[2,*] and Zeev Arad[1]

[1]*Department of Biology, Technion-Israel Institute of Technology, Haifa 32000, Israel* and [2]*Faculty of Aerospace Engineering, Technion-Israel Institute of Technology, Haifa 32000, Israel*

*Author for correspondence (e-mail: dweihs@tx.technion.ac.il)

Accepted 18 July 2005

Summary

Cormorants are water birds that forage by submerged swimming in search and pursuit of fish. Underwater they swim by paddling with both feet simultaneously in a gait that includes long glides between consecutive strokes. At shallow swimming depths the birds are highly buoyant as a consequence of their aerial lifestyle. To counter this buoyancy cormorants swim underwater with their body at an angle to the swimming direction. This mechanical solution for foraging at shallow depth is expected to increase the cost of swimming by increasing the drag of the birds. We used kinematic analysis of video sequences of cormorants swimming underwater at shallow depth in a controlled research setup to analyze the swimming gait and estimate the resultant drag of the birds during the entire paddling cycle. The gliding drag of the birds was estimated from swimming speed deceleration during the glide stage while the drag during active paddling was estimated using a mathematical 'burst-and-glide' model. The model was originally developed to estimate the energetic saving from combining glides with burst swimming and we used this fact to test whether the paddling gait of cormorants has similar advantages.

We found that swimming speed was correlated with paddling frequency (r=0.56, P<0.001, N=95) where the increase in paddling frequency was achieved mainly by shortening the glide stage (r=–0.86, P<0.001, N=95). The drag coefficient of the birds during paddling was higher on average by two- to threefold than during gliding. However, the magnitude of the drag coefficient during the glide was positively correlated with the tilt of the body (r=0.5, P<0.003, N=35) and negatively correlated with swimming speed (r=–0.65, P<0.001, N=35), while the drag coefficient during the stroke was not correlated with tilt of the body (r=–0.11, P>0.5, N=35) and was positively correlated with swimming speed (r=0.41, P<0.015, N=35). Therefore, the difference between the drag coefficient during the glide and during propulsion diminished at lower speeds and larger tilt. The mean drag of the birds for a single paddling cycle at an average swimming speed of 1.5 m s^{-1} was 5.5±0.68 N. The burst-and-glide model predicts that energy saving from using burst-and-glide in the paddling cycle is limited to relatively fast swimming speeds (>1.5 m s^{-1}), but that as the birds dive deeper (>1 m where buoyancy is reduced), the burst-and-glide gait may become beneficial even at lower speeds.

Key words: great cormorant, *Phalacrocorax carbo sinensis*, gait, paddling, burst-and-glide, drag, swimming.

Introduction

Hydrodynamic drag is a primary force in determining the performance of aquatic animals (Alexander, 1968). In a simplified form, it is the force (due to dynamic pressure differences over the body and skin friction) that causes the resistance to motion through the water. It sets limits to the maximum swimming speed achieved by the animal and has a direct effect on the energy expenditure during swimming (Bilo and Nachtigall, 1980; Hedenstrom and Liechti, 2001; Hui, 1988; Lovvorn, 2001; Lovvorn et al., 1991, 2001; Prange and Schmidt-Nielsen, 1970; Skrovan et al., 1999; Stelle et al., 2000; Stephenson, 1994; Thomas, 1996; Videler and Weihs, 1982; Webb, 1971; Weihs, 2002). At high Reynolds numbers Re ($Re=Ul/\upsilon$, where U is swimming speed, l is the length of the swimmer and υ is kinematic viscosity of water, ~10^{-6} m^2 s^{-1}), drag is proportional to size (area) and to the square power of the swimming speed (Hoerner, 1965). Drag is also dependent on shape. The latter is represented in the equation of drag in the form of a non-dimensional drag coefficient (C_d). The relation between C_d and drag force (at Re>10^4) is described as:

$$C_d = 2D/\rho A U^2 , \quad (1)$$

where D is drag, ρ is density of water (~10^3 kg m^{-3}) and A is a characteristic area.

C_d has been measured for different animals from models and carcasses in a water or air tunnel (Fish, 1984; Hui, 1988a; Lovvorn et al., 2001; Maybury and Rayner, 2001) or by using trained animals towed behind a boat (Williams and Kooyman, 1985). An indirect approach is to measure drag from the deceleration of live animals as they glide (Bilo and Nachtigall, 1980; Clark and Bemis, 1979; Miller et al., 2004; Stelle et al., 2000; Williams and Kooyman, 1985). This technique uses the fact that during the glide no thrust is being produced, hence the deceleration results directly from drag. By measuring the deceleration of the body, the drag force can be calculated from Newton's second law (F=Ma, where F=force, M=mass and a=acceleration). However, some correction is required for the added mass of water that is accelerated with the body (Vogel, 1994). The advantage of this technique is that the estimate is derived from animals swimming voluntarily, cruising at preferred speeds so that the shape and orientation of body parts is realistic. However, unlike with rigid objects, C_d of live animals changes during swimming. The swimming motions (undulations, flapping, rowing and paddling) increase the drag significantly beyond that of a motionless animal at the same swimming speed (Weihs, 1974; Schultz and Webb, 2002; Vogel, 1994). None of the above-mentioned techniques considers the elevated drag during active swimming and the drag measured is thus termed 'parasite drag' (for models and carcasses where the propelling appendages are removed) or 'passive drag' (for gliding animals). A different approach that does allow the estimation of the drag for active swimming is to model the thrust from the kinematics of the propelling appendages. Once thrust is estimated, then during swimming at constant speed, drag should equal thrust (Fish, 1993; Vogel, 1994). However, since estimation of passive drag from glides is relatively simple, it would be beneficial if active drag could be estimated directly from passive drag using simple kinematics. We explore this option using the swimming behavior termed 'burst-and-glide' (described by Weihs, 1974) that has been shown to exist in fish, marine mammals, penguins, water birds, lobsters, plankton and numerous aerial flyers (Haury and Weihs, 1976; Hove et al., 2001; Lovvorn, 2001; Sato et al., 2003; Spanier et al., 1991; Van Dam et al., 2002; Videler and Weihs, 1982; Webb and Fairchild, 2001; Weihs, 2002, 2004).

Swimming animals that use burst-and-glide can reduce the total energetic cost of swimming (Weihs, 1974; see Appendix). With this strategy, instead of swimming continuously at a constant speed, the swimmer accelerates to a final speed (U_f) above the desired average speed and then glides (decelerates) until reaching the initial speed (U_i). The energetic saving from such behavior is calculated as the ratio (R) between the energy required to burst-and-glide and the energy required to swim at the same average speed but at constant speed. R can be calculated directly from the burst-and-glide model using easily obtained kinematic data (see, for example, Videler and Weihs, 1982). However, the model requires knowledge of the parameter α, which is the ratio of drag during active swimming and drag during gliding. For example, the α used by Weihs (1974) for fish was 3, based on evidence that the drag of active swimming fish (dace and trout) is about three times the drag during passive gliding (Lighthill, 1971; Webb, 1971). A similar value of α was reported later for dolphins (Fish, 1993).

Cormorants propel their body underwater by stroking (paddling) with both feet simultaneously while the wings are tightly folded against the body (Lovvorn, 1991; Schmid et al., 1995). However, when swimming on the surface, cormorants employ alternate paddling, stroking with one foot at a time (Lovvorn, 1991; Ancel et al., 2000). Kinematic data on cormorants (*Phalacrocorax carbo sinensis* Blumelbach) swimming underwater (Ribak et al., 2004) showed that the paddling cycle is divided into three distinct successive stages: a stroke stage, where both feet move backward and generate the thrust; a glide stage, where the feet have no motion relative to the body; and a recovery stage, where the feet move forward relative to the body, in preparation for the next stroke. The glide stage lasts for approximately 50% of the entire paddling cycle duration (Ribak et al., 2004). The combination of a short power stage, where the birds accelerate, with a long glide stage, where the birds decelerate, resembles the burst-and-glide swimming pattern described above.

Submerged cormorants are positively buoyant (Lovvorn and Jones, 1991) so that the birds need to invest energy to remain submerged. Most of the buoyancy of water birds is due to air volumes in the plumage and in the airsacs (Lovvorn and Jones, 1991; Wilson et al., 1992), and their buoyancy therefore depends on diving depth. As the birds dive deeper, the hydrostatic pressure compresses the gas volumes, making the birds less buoyant. During shallow horizontal dives, cormorants swim with the midline of the body at an angle to the swimming direction (pitch, head pointing down, tail pointing up). This angle-of-attack generates hydrodynamic lift to help offset the positive buoyancy of the birds. This tilt of the body is highest during the stroke and recovery stages (Ribak et al., 2004). Using lift to counter buoyancy by tilting the body allows the birds to forage underwater at shallow depths where their buoyancy is maximal, but this behaviour should result in elevated drag during submerged swimming.

The drag coefficient (C_d) of the Brandt's cormorant *Phalacrocorax pencillatus* was measured by Lovvorn et al. (2001) by towing frozen, dead birds and a smooth featherless model. The values they obtained (based on the surface area as the characteristic area, A) were about 0.008 and 0.022 for the model and carcasses, respectively (at Re=10^6; figs 6 and 7 in Lovvorn et al., 2001). However, these values are applicable only for gliding birds at depths where buoyancy is negligible ($\geqslant$20 m; Wilson et al., 1992), since the towed birds were aligned in the direction of the flow and were not performing swimming motions. Great cormorants are shallow divers, mostly diving to depths <11 m (Grèmillet et al., 1999; Johansgard, 1993). Therefore, a method to estimate the drag during active paddling while taking into account the influence of buoyancy at shallow depths will provide a more realistic evaluation of the mechanical constraints on swimming for these waterbirds.

The problem of increased drag resulting from propulsive motions is a general issue confronting all animals that move in fluid media (air, water, biological fluids) and different species have found various ways of coping. Here we examine the adaptations of the cormorant, a flyer and also an adept swimmer. We use the long glide stage between the stroke and recovery stages in the paddling cycle of the cormorant to measure the passive drag of the birds from their deceleration. Then, we employ the 'burst-and-glide' model to calculate the drag of the bird during active swimming and to evaluate the energetic benefit of adding glides to the paddling cycle.

Materials and methods

Morphometric measurements

The calculation of C_d from deceleration requires a typical area (A, in Eqn 1) and added mass coefficients for the body of great cormorants *Phalacrocorax carbo sinensis* Blumelbach. We used volume V to the 2/3 power ($V^{2/3}$) for area, by calculating the volume of each bird from its body mass, and from the average density (810 kg m^{-3}) reported for cormorant carcasses (Ribak et al., 2004). An earlier study on parasite drag of cormorants reported drag coefficients based on surface area (Lovvorn et al., 2001), so we measured this area as well, to allow comparison (see below). Five carcasses of adult cormorants that were shot over fishing ponds during a wildlife management program were obtained fresh and stored frozen (–20°C) until processing after completely defrosting at room temperature (~15°C). The carcasses were used to estimate the added mass, surface area and general shape of the birds in three dimensions. This was done by folding the wings to their normal position during swimming, and securing them in place with tape. Each carcass was laid with its neck stretched on a 0.5 cm thick, 1×0.1 m plate, with markings every 1 cm along the long side of the plate. The tip of the bill, the tip of the tail and the center of the body were secured to the plate with tape. The plate with the bird was then advanced, 1 cm at a time, through a measuring device consisting of two perpendicular metal rods, sliding orthogonally with respect to each other (Fig. 1A). Each rod was scaled using a measuring tape (±1 mm), allowing the simultaneous measurement of height and width of the carcass each centimeter along the long axis of the body. The body is covered with soft plumage and has some flexibility, thus the measured height and width may change with the pressure applied by the measuring tool. To minimize this error, prior to each measurement the rods were pressed lightly onto the carcass and then released gently to allow the plumage and body tissues to push the rods back to normal position. The set of measurements from each carcass thus included diameters of 1 cm thick transverse 'slices' of the birds (Fig. 1B). The volume of each slice was calculated from the area of both sides of the slice, using the area of an ellipse (area = πyz, where y is half the height measurement and z is half the width measurement). Then, the area of both sides was averaged and multiplied by the thickness of the slice (1 cm) to obtain volume. The volumes of all the slices were summed to yield the total volume of the carcass. Similarly, surface area was measured from the perimeters of each side of the slices using the equation for an ellipse:

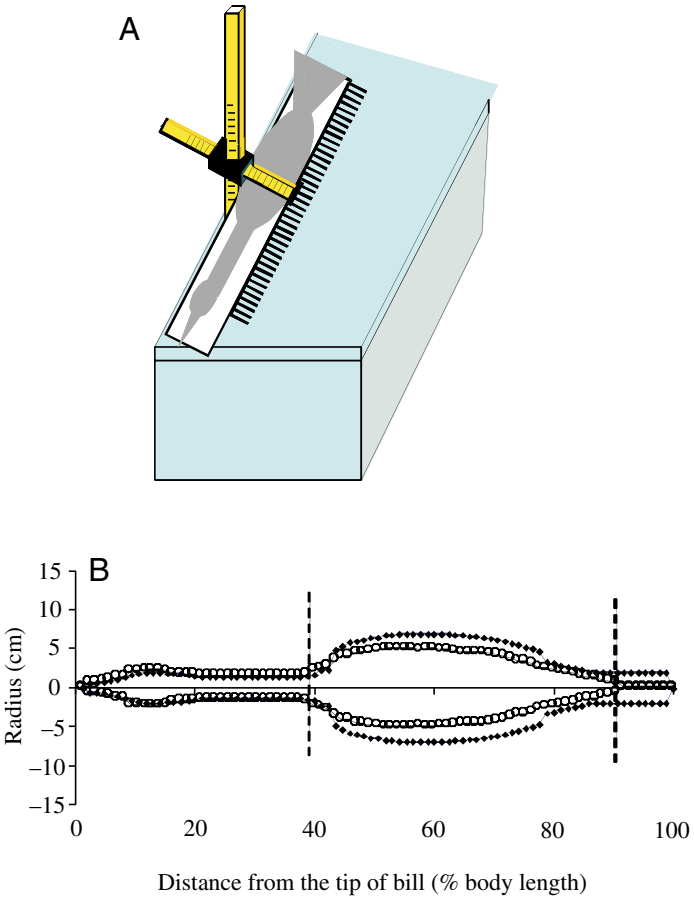

Fig. 1. Shape of the cormorant's body in three dimensions. (A) Schematic illustration (not to scale) of the apparatus used to measure the diameters of the cormorant carcass along the body's main axis. (B) Diameter of the width (lateral axis, solid rectangles) and height (dorso–ventral axis, empty circles). The x-axis represents the position along the body's main axis in % of body length (total body length = 85 cm). The diameters were used to calculate surface area, volume and added mass coefficients. The broken vertical lines mark the definition of the body excluding the neck and tail (trunk).

$$\text{Perimeter} = 2\pi\sqrt{\frac{y^2+z^2}{2}}\,. \qquad (2)$$

The surface area of each slice was assumed to be the average of both perimeters, multiplied by the slice thickness (1 cm). Then, all areas along the length of the bird were summed to yield the surface area of the whole bird. We divided the quantity $V^{2/3}$ of the carcasses by the measured surface area and used this ratio to convert C_d calculated based on $V^{2/3}$ to C_d calculated based on surface area in the live birds.

The added mass is the mass of water that is accelerated with a body and is proportional to the volume of the body (Denny, 1993). The exact magnitude of the C_d calculated from

decelerations depends slightly on the estimation of the added mass. Underestimation of the added mass will result in a lower calculated value of the drag coefficient and *vice versa*. To be as accurate as possible we estimated the added mass directly from the size and shape of the birds and accounted for the angle-of-attack θ of the body and tail. The added mass coefficient is the volume of the added mass divided by the volume of the body. An infinitely long cylinder moving parallel to its long axis has an added mass coefficient close to zero while the same cylinder moving perpendicular to its length will have an added mass coefficient of 1 (Lamb, 1945). Similarly the added mass of the body of the cormorant depends on whether it moves aligned in the direction of swimming (parallel to the length of the body) or if the body's main axis is tilted at an angle to the flow. Since the birds in our experiment were always gliding with their body at an angle-of-attack to the flow (tail pointing up) we obtained two added mass coefficients: once for the cormorant moving lengthwise and a second time for motion perpendicular to the longitudinal axis of the bird (θ=90°). The values of both were combined to estimate the added mass coefficient for a specific angle-of-attack. For the sake of this analysis we disregarded the neck, which contributes less than 10% to the volume of the entire body (9.5±1%, N=5), does not orient as the rest of the body, and therefore resembles a cylinder aligned with the direction of flow. We thus focused on estimating the added mass of the body (trunk) and tail. For the added mass coefficient relevant for lengthwise motion (C_{ax}) of the body we used 0.122, which is the theoretical value for a prolate spheroid with fineness ratio (length/diameter) of 3 (p. 155 in Lamb, 1945). For motion perpendicular to the flow (downwards) we used C_{ay}=1.339 (Table 1) for the body, which was the average calculated from our carcasses [standard error of mean (S.E.M.)=0.045, N=5] using elongated body theory (see, for example, Lighthill, 1970, 1960). The theory states that the added mass of each cross section of a slender body moving broadside to the flow is approximately the volume of a cylinder with a circular cross section that encompasses the diameter of the body at the specific cross section. Thus using the diameters of the body measured at each 1 cm along its length (excluding the neck and tail), we calculated the volume of encompassing cylinders (1 cm long) and integrated all volumes to achieve the volume of added mass when the body is tilted at θ=90°.

The volume of added mass was then divided by the actual volume of the bird to yield the added mass coefficient for motion perpendicular to the flow (C_{ay}). The specific added mass coefficient for a given θ was assumed to be the sum of the projections of the two added mass coefficients (C_{ax} and C_{ay}) on the direction of swimming:

$$C_{a(\theta)} = C_{ax}\cos\theta + C_{ay}\sin\theta \, . \quad (3)$$

The same approach was used for the tail, treating it as a flat plate with trapezoid shape and dimensions of 2 cm and 8.6 cm at the bases and 13.8 cm as the length (data taken from Ribak et al., 2004, which described the planform area of tails of cormorants during swimming). For such a plate C_{ax} is negligible (C_{ax}=0) and C_{ay} is the volume of a truncated cone with radii 1 cm and 4.3 cm at the bases and height 13.8 cm (=3.44×10^{-4} m^3) divided by the volume of the bird. The added mass coefficient $C_{a(\theta)}$, for the tail is calculated as in Eqn 3 but using the angle-of-attack of the tail (the angle between the upper surface of the tail and the direction of swimming). Calculating separate added mass coefficients for the body and tail enabled us to account for changes in the added mass of the bird due to changes in the angle-of-attack of the body and of the tail when the two were not the same. Finally the added mass coefficient C_a of the entire bird (body and tail) is the sum of the coefficients ($C_{a(\theta)}$) for the tail and for the body.

Body length (tip of bill to tip of tail) of the live birds used to calculate the Reynolds number was measured from scaled images of the birds swimming with their neck stretched.

Swimming sequences

Video sequences were obtained from 5 male and 5 female adult (age >3 years) great cormorants swimming in an experimental setup described previously (Ribak et al., 2004). The birds were filmed swimming inside a straight, 7 m-long metal mesh channel, with a rectangular 0.5 m×0.5 m profile,

Table 1. *Volume and surface area of great cormorant carcasses*

Carcass	Body mass (kg)	$V\times10^{-3}$ (m^3)	A_w (m^2)	$V^{2/3}/A_w$	C_{ay}
G022	2.220	3.105	0.158	0.134	1.298
G020	2.376	3.181	0.162	0.134	1.220
G019	2.028	2.816	0.155	0.128	1.480
G017	2.178	2.924	0.160	0.128	1.397
G016	2.159	2.810	0.155	0.129	1.299
Mean ± S.E.M.	2.192±0.056	2.97±0.07	0.158±0.0013	0.131±0.001	1.339±0.045

V, volume; A_w, surface area; N=5.

The measurement of volume was used to estimate the added mass coefficient and the surface area was used to calculate a conversion ratio between C_d based on $V^{2/3}$ and C_d based on surface area ($V^{2/3}/A_w$).

C_{ay} is the added mass coefficient of the body (trunk) for motion perpendicular to its longitudinal axis (θ=90°) calculated from elongated body theory (see text).

placed on the floor of a 1 m-deep pool. A 2 m-long section in the tunnel, starting 3.5 m away from the entrance, was used as a testing section. It was equipped with a mirror (2 m×0.7 m) angled at 45° above the tunnel. The birds were filmed swimming in the test section using a CCTV video camera (VK-C77E, Hitachi, Tokyo, Japan; 752×582 effective pixels, shutter speed 1/50s), inside an underwater housing, and connected to a S-VHS video (HR-S7600AM, JVC, Tokyo, Japan). The camera was positioned 0.5 m above bottom, 2 m away from the middle of the testing section, and covered most of the testing section and the mirror (2.3 mm/pixel in the side view 2.7 mm/pixel in the upper view, 0.0030–0.0036 body length/pixel, respectively), thus allowing simultaneous lateral and dorsal (through the mirror) views of the swimming bird while using a single camera. The video sequences (each containing one complete paddling cycle) were converted to consecutive video fields (50 fields s^{-1}, i.e. time resolution was ±0.02 s) using a video editing system (Edit 6, Autodesk Inc., San Rafael, CA, USA).

The position of the test section along the tunnel was chosen to allow sufficient distance for the birds to develop a repeated burst-and-glide cycle at given average swimming speed in a straight path prior to the measurement of swimming parameters. The tunnel was positioned along the floor at the center of the pool, at least 1 m away from the nearest wall. We calculated the ground effect (Hoerner, 1975) on the cormorants and found it to be negligible beyond a distance of one body thickness (maximum distance between dorsal and ventral sides of the body) from the floor (at $Re>10^6$) and hence only used runs that were >10 cm distant from the floor. The upper 0.5 m height limitation of the tunnel ensured that the birds were swimming away from the surface, at a distance of more than 4 times the body thickness. Hence, no surface waves formed by the swimming bird were measured and the resulting added drag can be assumed to be negligible (approaching zero at depth >3 times the body thickness; fig. 289 in Hertel, 1966).

Only a few minutes each time (<10 min) were required to obtain 5–8 video sequences from each bird in a series of 4 sampling days. The short duration of the experiments ensured that changes in buoyancy due to time-dependant plumage wettability would be small (Ribak et al., 2005).

Kinematic analysis

In each sequence, stride length was defined as the horizontal distance traversed during the paddling cycle. The cycle duration was calculated from the number of video fields per cycle and paddling frequency was defined as (cycle duration)$^{-1}$. The average swimming speed for the entire cycle was defined as stride length divided by cycle duration. Each paddling cycle was divided into three distinct stages: stroke, glide and recovery, based on the motion of the feet as described above and in Ribak et al. (2004). The changes in gait during swimming were analyzed by testing for correlation between the duration of each of the three stages with paddling frequency.

The upper view (through the mirror) in each video field was used to measure the instantaneous speed of the birds. This was done by measuring in each video field the position of a small, round (1.5 cm in diameter) tag glued to the feathers on the back of the birds. The momentary horizontal swimming speed was calculated as the first derivative ($\partial x/\partial t$) of the function describing the change in position along the x (horizontal) axis with time, using a Lagrange 3-points numerical equation (Hildebrand, 1956). In each paddling cycle, the birds had slight vertical deviations (~2 cm) from the horizontal direction (Ribak et al., 2004). However, the descent and ascent angles (measured from the side view) were sufficiently small (~4°) that the horizontal component of the measured speed represents over 99% of the two-dimensional speed. The angle-of-attack of the body during the glide was defined as the angle between the longitudinal midline of the body (base of neck to base of tail) and the instantaneous direction of swimming in the side view.

The velocity profiles, each comprising one complete paddling cycle (Fig. 2), were used for analysis of drag and burst-and-glide. During the stroke, the body accelerates, and during the glide and recovery it decelerates. Following Weihs

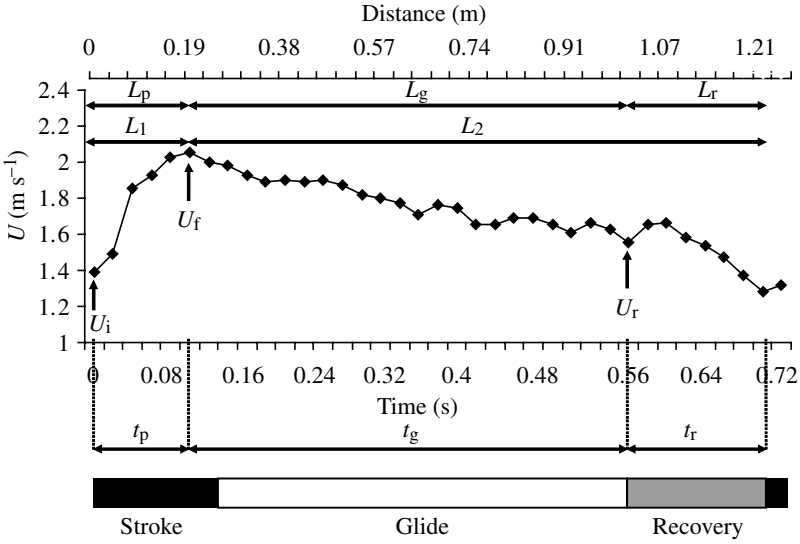

Fig. 2. Variation in velocity during one paddling cycle. The plot was obtained from one video sequence (Bird 5) and smoothed by a stepwise 5-point moving average for easy viewing. The plot shows the kinematic parameters defined by Weihs (1974) for the burst-and-glide model (L_1, L_2, U_i, U_f), and the additional parameters defined in the present study (L_p, L_g, L_r, U_r, t_p, t_g, t_r); see List of symbols for the description of each parameter. The bottom bar indicates the division of the paddling cycle into three stages based on the motion of the feet relative to the body (stroke, glide and recovery). Average swimming speed for this cycle was 1.72 m s^{-1}. Note that the bird did not swim at a constant speed but rather accelerated during the power stage and decelerated during the glide and recovery stages in a burst-and-glide swimming pattern.

(1974), we defined a parameter U_f as the maximum instantaneous speed of the body during the stroke, and U_i as the minimum speed at the start of the stroke. The time interval between them was defined as the power stage (t_p, see Fig. 2) to differentiate it from the stroke stage, which is a more robust kinematic definition based solely on the motion of the feet. The speed at the start of the recovery stage was defined as U_r and t_g was defined as the duration of the deceleration from U_f to U_r. t_r was the duration of the recovery stage. We measured L_p, L_g and L_r as the horizontal distances traversed during the power (t_p), glide (t_g) and recovery (t_r) stages, respectively (L_p+L_g+L_r=stride length).

Stride length, paddling frequency and average swimming speed were measured from all the sequences available (95 sequences from 10 birds). However, for the calculation of the drag coefficients we used only the best 35 sequences (from 10 birds) that had the same speed at the start and at the end of the cycle and the smoothest velocity profiles, with distinct acceleration and deceleration. In a few cases, data smoothing, using 3 or 5 point stepwise moving averages, was necessary to determine the exact point of transition between t_p and t_g,on the velocity profiles. The sequences used were the ones where the birds were swimming as straight as possible (no sideslips and minimal vertical deviations of the center of mass).

Estimation of drag

The instantaneous speed profiles from each of the 10 birds were used to evaluate the drag coefficients of the birds, both when actively swimming and during gliding. We assumed that during the glide and recovery stages, the body moves due to inertia, and thrust is not added to the system so that the C_d of the glide and recovery can be calculated directly from the deceleration of the birds. This assumption is trivial for the glide stage, but in the recovery stage, the forward motion of the feet may presumably add some forward thrust (from inertia). Here we assume that this thrust is negligible since it is likely cancelled by the increased drag on the feet, as they move against the swimming direction. The velocity profiles indicate that the birds indeed decelerated during the recovery stage (Fig. 2).

For the calculation of the drag coefficient during the glide stage we used the technique suggested by Bilo and Nachtigall (1980), based on the average linear slope (C) of the inverse instantaneous speed (U^{-1}) *vs* time:

$$C_d = \frac{2Cm}{\rho A} . \quad (4)$$

where C is the slope of the least-square linear regression between U^{-1} and time (obtained from the glide data), m is the virtual mass of the birds (bird mass + added mass; Stelle et al., 2000), A is taken as volume of the bird to the 2/3 power, and ρ is water density (10^3 kg m^{-3}). Virtual mass (m) is calculated from the mass of the bird (M) in kg, the added mass coefficient calculated for the bird in the mean angle-of-attack during the glide (C_a,,see morphometric measurements) and the volume of the bird (V) in m^3. It is thus calculated as:

$$m = M + \rho V C_a . \quad (5)$$

The calculations of C_d were made once for the glide stage ($C_{d,glide}$) and then for the combined glide + recovery stage ($C_{d,glide+recovery}$). After $C_{d,glide}$ and $C_{d,glide+recovery}$ are calculated, the C_d for the recovery stage ($C_{d,recovery}$) can be isolated either directly from the kinematic data of the deceleration during the recovery, or arithmetically, treating the $C_{d,glide+recovery}$ as the mean contribution of the $C_{d,glide}$ and the $C_{d,recovery}$ combined:

$$C_{d,glide+recovery} = C_{d,glide}\left(\frac{L_g}{L_g+L_r}\right) + C_{d,recovery}\left(\frac{L_r}{L_g+L_r}\right), \quad (6)$$

where $C_{d,glide+recovery}$ and $C_{d,glide}$ were calculated from Eqn 4 above, and the distances L_g and L_r are taken from the kinematic data.

We can now use the burst-and-glide model to calculate C_d for the burst (power) stage ($C_{d,stroke}$). The burst-and-glide model is based on a two-stage swimming behavior. It defines L_1 as the distance traveled during the acceleration (burst) and L_2 as the distance traveled during the deceleration and provides equations to calculate each of them from U_i and U_f (see Appendix). We used the fact that L_1 and L_2 can be measured directly from the kinematic data to solve these equations for α in the burst-and-glide model. The factor α is the ratio between the drag coefficient during the burst stage and the drag coefficient during the glide. We replaced L_2 in the original calculation with our L_g+L_r and used L_p instead of the original L_1. The modified equations are therefore:

$$\frac{L_g+L_r}{L_p} = \frac{\alpha \ln(U_f/U_i)}{\ln(\cosh B + \overline{U_i}\sinh B)} , \quad (7)$$

where

$$B = \tanh^{-1}\frac{\overline{U_f}-\overline{U_i}}{1-\overline{U_f}\,\overline{U_i}} , \quad (8)$$

where $\overline{U_i}$=U_i/U_e and $\overline{U_f}$=U_f/U_e; U_e is a reference velocity, chosen, for convenience, to be larger than the highest measured velocity so that the normalized values are always <1. Weihs (1974) called this speed the maximum achievable sustained swimming speed.

The factor α may now be isolated from Eqn 7 and solved using the values of L_p, L_g, L_r, U_i, U_f and U_e. Except for the latter, all parameters are available from the kinematic data. For U_e we used the value 2.5 m s^{-1}, which was slightly higher than the maximum U_f observed in our data (2.41 m s^{-1}). Once α is obtained, the C_d of the power stage ($C_{d,stroke}$) can be obtained from the definition of α:

$$\alpha = \frac{C_{d,stroke}}{C_{d,glide+recovery}} , \quad (9)$$

where $C_{d,glide+recovery}$ was obtained from Eqn 4.

We now have the drag coefficient for each of the stages (stroke, glide and recovery). To calculate the instantaneous drag force (at $Re>10^5$) from the drag coefficients at any point in time along the cormorant paddling cycle, one needs to substitute the appropriate C_d and instantaneous speed (U) into Eqn 1 and isolate D as:

$$D = \tfrac{1}{2}\rho C_d A U^2 . \quad (10)$$

The average drag for the entire paddling cycle is the integral of Eqn 10 over time, divided by the paddling cycle duration:

$$D = \tfrac{1}{2}\rho A \left(\frac{\int_0^{t_p} C_{d,stroke} U^2 dt + \int_{t_p}^{t_p+t_g} C_{d,glide} U^2 dt + \int_{t_p+t_g}^{t_p+t_g+t_r} C_{d,recovery} U^2 dt}{t_p+t_g+t_r} \right), \quad (11)$$

where t_p, t_g and t_r are the durations of the power glide and recovery stages, respectively (Fig. 2).

The burst-and-glide model was developed to evaluate the energetic advantage of using burst-and-glide. If we continue to solve the original model we can obtain the energetic advantage (R) of combining glides in the paddling cycle, as opposed to constant paddling at constant swimming speed, from the following equations (modified from Videler and Weihs, 1982; see Appendix):

$$\overline{U_c} = \frac{\alpha \ln(U_f/U_i) + \ln(\cosh B + \overline{U_i}\sinh B)}{B + \alpha\,(1/\overline{U_i} - 1/\overline{U_f})} , \quad (12)$$

$$R = \left(\frac{1}{\overline{U_c}^2}\right) \times \left(\frac{1}{1+[(L_g+L_r)/L_p]}\right) . \quad (13)$$

R is the ratio of the energy expended during burst-and-glide *vs* the energy expended for swimming constantly at the same average speed. In the case where there is no benefit in gliding R=1, and as R becomes smaller, the energetic advantage in burst-and-glide, as opposed to swimming at constant speed, will be greater. However, in our specific case, simply solving for R will result in an exaggerated value. This is because we combined the recovery stage with the glide for the drag estimation. The α value that we calculated above (as a means to find $C_{d,stroke}$) considers only the stroke stage as 'active swimming', while in practice, the recovery stage is part of the active swimming as well. To find α that is relevant for the calculation of the energetic advantage in combining glides into the paddling cycles that contain only stroke and recovery, we repeated the analysis, this time with the recovery included in the burst stage of the burst-and-glide model.

We defined a new drag coefficient for the stroke + recovery stages ($C_{d,propulsion}$) and recalculated α (Eqn 7), this time replacing L_1 with (L_p+L_r), and U_i with U_r (the velocity at the beginning of the recovery stage). The above mentioned Eqn 7 and 8 then become:

$$\frac{L_g}{L_p+L_r} = \frac{\alpha \ln(U_f/U_r)}{\ln(\cosh B + \overline{U_r}\sinh B)} , \quad (14)$$

and

$$B = \tanh^{-1} \frac{\overline{U_f} - \overline{U_r}}{1 - \overline{U_f}\,\overline{U_r}} , \quad (15)$$

where $\overline{U_r}$=U_r/U_e.

The new α obtained is defined as:

$$\alpha = \frac{C_{d,propulsion}}{C_{d,glide}} . \quad (16)$$

We then continue to use the burst-and-glide model, replacing L_1 in the original model with (L_p+L_r), and U_i with U_r. Thus, Eqn 12 and 13 above become:

$$\overline{U_c} = \frac{\alpha \ln(U_f/U_r) + \ln(\cosh B + \overline{U_r}\sinh B)}{B + \alpha(1/\overline{U_r} - 1/\overline{U_f})} , \quad (17)$$

and

$$R_p = \left(\frac{1}{\overline{U_c}^2}\right) \times \left(\frac{1}{1+[L_g/(L_p+L_r)]}\right) . \quad (18)$$

This R_p is the energetic saving, adjusted for the special case of three-stage paddling. It gives the ratio of the energy required for a paddling cycle including a glide *vs* the energy needed to swim constantly at the same average swimming speed, with a paddling cycle that includes only stroke and recovery.

Data analysis

Thirty five sequences (from ten different birds) were fully analyzed for the drag coefficients and burst-and-glide parameters (R, R_p) while a larger sample size was used to analyze gait, paddling frequency and stride length (95 sequences). Statistical significance for correlations between variables was tested using Statistica (StatSoft, Tulsa, OK, USA). To ensure no bias from pseudo-replications or the unequal number of trials per bird, statistical significance of all correlations that are reported here for all the trials were tested a second time using mean values per bird (N=10 birds). Similarly, the mean values reported throughout this work are the means of all birds (N=10), calculated by averaging all values from sequences from a single bird and then averaging for all birds. Values of statistical variation quoted in the text and figures are thus standard error of mean (S.E.M.) where N=10 birds. Tables 2 and 3 are an exception. These tables present the means of each bird calculated from small and unequal sample size. We therefore chose to present variance in these tables as the standard deviation (S.D.).

Results

The morphometric measurements performed on carcasses are summarized in Table 1.

The swimming speed of the cormorants in the video sequences was 1.51±0.058 m s^{-1} (N=10 birds). Mean swimming speed calculated for each bird in the experiment (Fig. 3) was correlated with the bird's body mass (r=0.75, P<0.015, N=10) and body length (r=0.87, P<0.015, N=10). The paddling frequency was positively correlated with swimming speed (r=0.56, P<0.001, N=95 sequences). This was achieved mainly by shortening the duration of the glide stage as the paddling frequency increased (r=–0.86, P<0.001, N=95 sequences) while the duration of the stroke and recovery stages remained unaffected (stroke: r=0.009, P>0.93; recovery: r=0.035, P>0.74) (Fig. 4A). Taking this into account, the relation between the duration of the glide stage and the paddling frequency suggests a maximal paddling frequency of approximately 2.7 Hz when glide duration is zero (Fig. 4A,B).

Table 2 summarizes the kinematic data used for the drag estimation and Table 3 summarizes the various drag coefficients, R and R_p,calculated from the model. The Re for each bird, based on body length and average speed (Table 3), ranged between 0.9×10^6 and 1.4×10^6 (mean= $1.12\times10^6\pm5.92\times10^4$). The average $C_{d,glide}$ calculated for each bird, using $V^{2/3}$ as a reference area, was 0.143±0.011 (N=10 birds), but ranged between a minimum of 0.091 to a maximum of 0.180. The $C_{d,glide}$ calculated for each sequence was negatively correlated with the Re and mean swimming speed calculated for the same sequence (r<–0.62, P<0.001, N=35 in both cases). When the average $C_{d,glide}$ for each bird was compared with the average Re (or the average speed) for the same bird (giving equal weight to all birds) the correlation improved (r<–0.93, P<0.001, N=10). Each $C_{d,glide}$ obtained from a video sequence was positively correlated with the average angle-of-attack of the body during the glide in that sequence (r=0.50, P<0.003, N=35). A similar relation between the average angle-of-attack during the stroke and $C_{d,stroke}$ was not significant (r=–0.11, P>0.54, N=35 sequences). The average angle-of-attack during the glide was negatively correlated to the average swimming speed (r=–0.65, P<0.001, N=35), so while swimming faster the birds were swimming at smaller angle-of-attack and *vice versa*. The average angle-of-attack during the stroke stage was not significantly correlated to the average swimming speed (r=–0.29, P>0.09, N=35) or to the average swimming speed during the stroke phase (r=–0.21, P>0.22, N=35). $C_{d,stroke}$ was positively correlated with the average swimming speed (r=0.41, P<0.015, N=35).

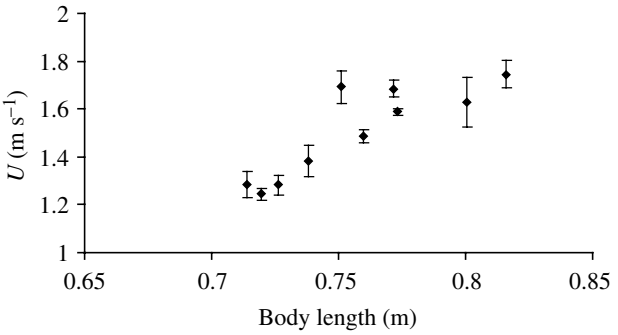

Fig. 3. The average swimming speed observed for each cormorant in the experiment relative to body length. Each point is the mean swimming speed obtained from 5–10 sequences taken of the same bird (values are ± S.E.M.).

The average $C_{d,recovery}$ and the $C_{d,stroke}$ were 0.273±0.054 and 0.432±0.040 respectively (N=10 birds). The average $C_{d,recovery}$ and $C_{d,stroke}$ for each bird were 2.6±0.71- and 3.2±0.57-fold higher, respectively, than $C_{d,glide}$ of the same bird (N=10). The average drag for the entire paddling cycle (as calculated from Eqn 11) for each bird was 5.5±0.68 N (N=10). The drag was highest during the stroke, then decreased considerably during the glide, and increased slightly during the recovery stage (Fig. 5). The burst-and-glide model predicts an average R_p value of 0.99±0.077 and a R value of 0.68±0.078 (Table 3). Thus, when the recovery stage is considered as part of the

Table 2. *Kinematic data from the swimming sequences of the great cormorant*

Bird	U (m s^{-1})	N	L_p (m)	L_g (m)	L_r (m)	U_i (m s^{-1})	U_f (m s^{-1})	U_r (m s^{-1})	t_p (s)	t_g (s)	t_r (s)
1	1.43±0.169	4	0.186±0.009	0.585±0.072	0.164±0.040	1.28±0.39	1.69±0.099	1.13±0.129	0.17±0.048	0.35±0.118	0.17±0.020
2	1.75±0.182	2	0.229±0.069	0.541±0.016	0.217±0.081	1.29±0.43	2.13±0.266	1.87±0.284	0.12±0	0.25±0.014	0.15±0.042
3	1.31	1	0.191	0.472	0.216	0.55	1.98	1.37	0.12	0.24	0.24
4	1.68±0.092	4	0.224±0.020	0.549±0.164	0.262±0.029	1.42±0.12	1.98±0.232	1.48±0.237	0.13±0.034	0.205±0.030	0.2±0.023
5	1.62±0.230	5	0.207±0.029	0.685±0.098	0.158±0.026	1.41±0.27	1.89±0.330	1.52±0.284	0.14±0.046	0.38±0.071	0.14±0.022
6	1.71±0.027	5	0.237±0.009	0.868±0.049	0.142±0.015	1.34±0.10	2.09±0.132	1.49±0.250	0.13±0.023	0.48±0.026	0.11±0.011
7	1.47±0.047	3	0.195±0.010	0.314±0.159	0.009±0.525	1.32±0.21	1.65±0.092	1.55±0.136	0.14±0.02	0.19±0.081	0.15±0.012
8	1.40±0.064	5	0.163±0.539	0.567±0.133	0.184±0.09	0.90±0.22	1.61±0.200	1.19±0.159	0.14±0.017	0.40±0.121	0.20±0.080
9	1.30±0.058	4	0.170±0.010	0.578±0.233	0.152±0.049	0.97±0.08	1.37±0.308	1.09±0.172	0.15±0.026	0.45±0.126	0.15±0.026
10	1.62±0.008	2	0.209±0.002	0.509±0.046	0.198±0.029	1.15±0.11	2.15±0.242	1.58±0.177	0.12±0	0.24±0	0.15±0.014

Listed are the parameters used as input in the burst and glide model (see List of symbols and Fig. 2 for descriptions of the parameters). Each parameter is the mean ± S.D. of all the sequences analyzed from the same bird (N = number of sequences per bird).

glide, the average energetic gain of the birds from the non-constant swimming speed is 32%. However, if the recovery is considered as part of the burst stage, then on average there is no energetic saving from using burst-and-glide. The values of R and R_p were negatively correlated with the average swimming speed (r<–0.68; P<0.001; N=35 for both R and R_p), suggesting that the faster birds were gaining more from burst-and-glide while the slower birds were actually losing from it relative to an idealized constant swimming (Fig. 6A). The α calculated from the burst-and-glide model (using Eqn 7 or 14) increased non-linearly with the increase in swimming speed (Fig. 6B). At low speeds, α was close to 1 and then increased sharply up to 8 in the fastest birds.

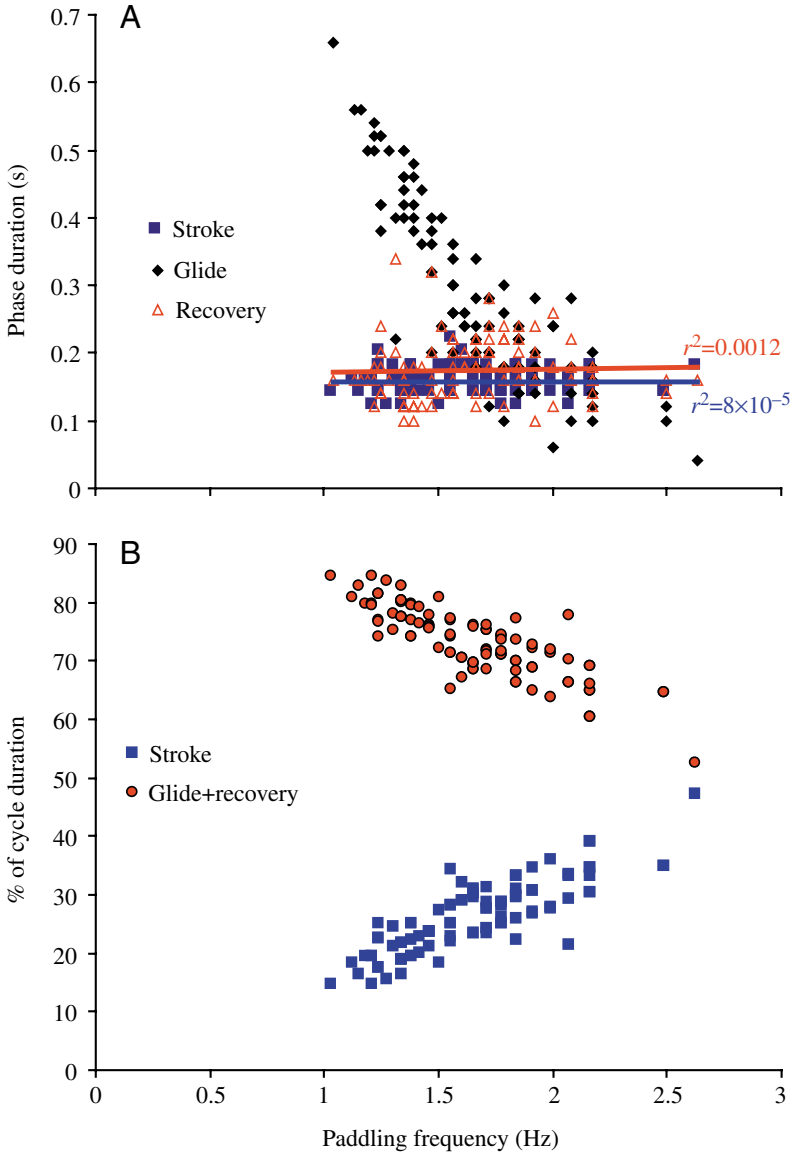

Fig. 4. The duration of each stage in the paddling cycle of the great cormorant (A) and the proportion of the power (burst) and deceleration (glide + recovery) stages in the paddling cycle (B) in relation to paddling frequency. Note that the glide duration decreased with the increase in paddling frequency. At a paddling frequency of 2.7 Hz, the duration of the glide phase was diminished to almost zero so that the power and recovery stages each occupy ~50% of the paddling cycle duration.

Discussion

The present study shows that in order to swim faster, cormorants shorten their paddling cycle by shortening the duration of the glide stage within each cycle. Clark and Bemis (1979) reported a similar trend in penguins and suggested that this either allows the propelling muscles to operate at maximum efficiency over a range of swimming speeds or allows an energy saving from burst-and-glide swimming. In the case of the cormorant, an additional advantage is derived from the fact that the recovery stage occurs when the speed of the body is minimal. Thus, the increase in the drag coefficient during the recovery stage is compensated for by the lower swimming speed at the end of the paddling cycle, maintaining a relatively low drag (Fig. 5).

During the glide, the body is at the smallest angle-of-attack, the neck is aligned with the swimming direction, and the feet are trailing behind the body. At this posture, the bird can optimally use its momentum to keep moving at relatively low drag. During propulsion (stroke and recovery), the tilt of the body is increased and the feet are moved from their posterior position under the tail. This results in an increase in the drag coefficient, and thus the drag of active swimming is higher than during gliding. The duration of the paddling cycle is determined by the length of the glide stage. When paddling frequency increases, propulsion occupies a more significant portion of the paddling cycle (Fig. 4B) and this affects the drag of the bird. Therefore, the ability to calculate a drag coefficient for each stage of the swimming cycles, using simple kinematics, allows the more accurate calculation of the drag during swimming for a wide range of paddling cycles that combine glides and propulsion.

While the drag coefficient for the glide stage was lower than the drag coefficient for the recovery and stroke stages, its value was affected by the need to counter buoyancy. Cormorants are positively buoyant and use hydrodynamic lift to counter their tendency to float while swimming underwater (Ribak et al., 2004). The magnitude of the lift force is dependent on swimming speed and on the angle-of-attack of the body. We show here that the birds that were swimming slower had higher drag coefficients for the glide stage. This is because the slower birds tilted their body at a larger angle-of-attack to compensate for the reduced speed and achieve sufficient lift to counter their buoyancy. This tilt increased their drag coefficient, as evident from the significant correlation between $C_{d,glide}$ and the tilt of the body. Thus, the actual drag encountered by cormorants

Table 3. *The calculated drag coefficient for each stage of the paddling cycle of the great cormorant and the resulting average drag per cycle*

Bird	Mass (kg)	Length (m)	$Re\times10^6$	R_p	R	$C_{d,glide}$	$C_{d,recovery}$	$C_{d,stroke}$	Drag cycle^{-1}
1	1.99	0.74	1.04	1.22±0.16	0.62±0.21	0.176±0.145	0.030±0.353	0.339±0.041	4.3±0.14
2	2.30	0.82	1.41	0.73±0.20	0.55±0.27	0.101±0.031	0.476±0.230	0.711±0.233	10.6±2.05
3	1.89	0.73	0.94	1.04	1.26	0.180	0.565	0.394	5.2
4	2.10	0.79	1.32	1.01±0.20	0.50±0.13	0.120±0.043	0.201±0.097	0.556±0.418	7.4±4.35
5	2.40	0.77	1.24	0.80±0.15	0.49±0.16	0.124±0.026	0.183±0.103	0.480±0.164	6.0±2.02
6	2.18	0.77	1.31	0.62±0.12	0.43±0.04	0.091±0.017	0.122±0.104	0.411±0.135	4.7±1.06
7	2.00	0.76	1.11	1.31±0.19	0.80±0.23	0.166±0.087	0.189±0.085	0.287±0.211	4.07±2.90
8	1.48	0.72	1.00	1.22±1.24	0.82±0.22	0.180±0.041	0.423±0.256	0.373±0.104	3.2±0.55
9	1.80	0.71	0.92	1.16±0.32	0.74±0.58	0.171±0.025	0.343±0.289	0.325±0.083	3.5±0.9
10	1.90	0.75	1.21	0.79±0.02	0.57±0.03	0.119±0.061	0.194±0.243	0.441±0.007	5.6±1.00
Mean ± S.D.	2.004±0.263	0.76±0.03	1.12±0.172	0.99±0.242	0.68±0.246	0.143±0.035	0.273±0.171	0.432±0.126	5.5±2.16

$C_{d,glide}$, $C_{d,recovery}$ and $C_{d,stroke}$ are the drag coefficients during the glide, recovery and stroke stages, respectively (see text for the description of the stages).

Also listed are the dimensions of the birds: mass used to estimate the area of the birds ($V^{2/3}$) and length used in the calculation of the Reynolds number (Re) for the swimming cycle, Re=(length$\times U$)/ν, where U is the average swimming speed for a paddling cycle. R_p and R are the energy ratios in the burst and glide model, where R_p is calculated with the recovery stage as part of the burst stage and R is calculated with the recovery stage as part of the glide stage.

Values listed are the means for each bird ± S.D. The sample size for each bird is as listed in Table 2.

swimming at shallow depths is greatly affected by the need to counter buoyancy. Buoyancy is considered the primary mechanical constraint of diving water birds, but this constraint is depth-dependent (Wilson et al., 1992; Lovvorn and Jones, 1991). Here we show that although the birds have managed to cope with the mechanical constraint of buoyancy during shallow submerged swimming, there exists an energetic trade-off in which the birds are required either to swim faster or swim at a larger angle-of-attack, increasing the drag in either case and thus making shallow foraging more costly.

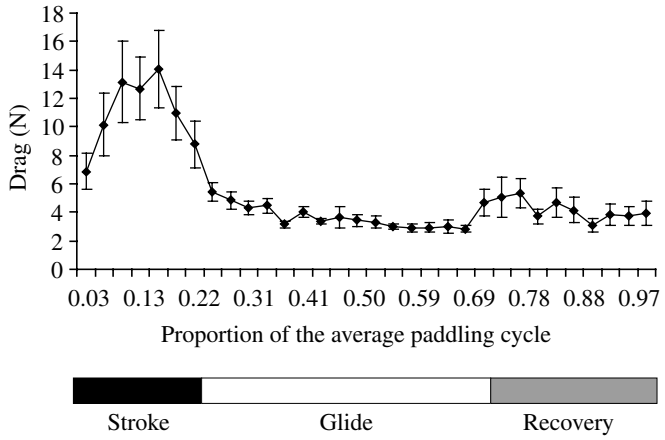

Fig. 5. The distribution of the momentary drag along an average paddling cycle of the great cormorant. Momentary drag is calculated using the C_d average for each of the paddling stages. To average all the analyzed sequences despite the differences in cycle duration, the x-axis is the proportion of the cycle duration that is normalized by dividing the period of each stage (stroke, glide and recovery) by the mean duration of that stage. To allocate equal weight to all birds, the sequences of each bird were first averaged and then means ± S.E.M. of all birds were calculated.

Unlike in the glide stage the $C_{d,stroke}$ was not statistically correlated with the average angle-of-attack of the body during the stroke. This may be due to the fact that the angle-of-attack changes throughout the stroke stage while our $C_{d,stroke}$ is an average for the entire stage. Another explanation is that during the stroke the tail changes orientation and the feet move beneath the body, thus changes in the drag coefficient during propulsion are not limited to the increase in the angle-of-attack. $C_{d,stroke}$ was, however, positively correlated with the average swimming speed. Thus as swimming speed increased, $C_{d,glide}$ decreased while $C_{d,stroke}$ increased, and this resulted in the increase in α observed here (Fig. 6B).

The birds in our study differed only slightly in body length (0.71–0.82 m), and to a greater extent in average swimming speed (1.3–1.75 m s^{-1}). Hence the variation in Re between birds was mainly due to the difference in swimming speeds. Re was negatively correlated with $C_{d,glide}$. Such a relation may be due to a reduction in the thickness of the boundary layer (Hoerner, 1965). In our case, however, it is more likely that the decrease in $C_{d,glide}$ with speed is due to the above-mentioned need to tilt the body further during slow swimming. Regardless of the precise reason for the decrease in $C_{d,glide}$ at higher Re, this relationship explains why each of our birds had a fairly distinct swimming speed (Fig. 3) that was correlated with body size. The average thrust for a complete cycle, developed by each bird, should equal its drag. If we assume that the thrust developed by each bird during the paddling is proportional to the bird's size (i.e. thrust/A=constant), then the birds should glide at similar values of $C_{d,glide}U^2$. Multiplying the square of the average swimming speed and the average

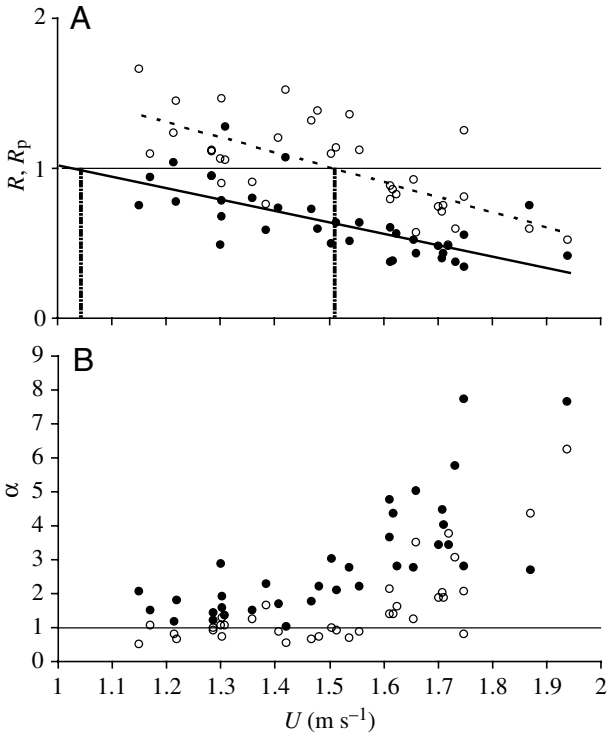

Fig. 6. The 'burst-and-glide' parameters R or R_p (A) and α (B) in relation to the average swimming speed of the great cormorant in each paddling cycle. Open symbols denote calculated values when the recovery is treated as part of the burst stage and full symbols are calculated values when the recovery is treated as part of the glide stage (see text). Solid horizontal lines mark the proportion of 1, where the energetic cost of burst-and-glide is exactly the same as for swimming at constant speed. Broken vertical lines in A mark the threshold average speed where the least square regression of the points (broken line for R_p, solid line for R) intersects with the value of 1. At this swimming speed the energetic benefit from burst-and-glide changes from gain (R<1) into loss (R>1). In B, values ⩽1 imply that the drag coefficient for passive drag is as high as or higher than the coefficient for active swimming. Note that the open symbols represent a more conservative approach for estimating the energetic advantage from burst-and-glide.

$C_{d,glide}$ obtained for each bird yields a constant value (0.309±0.0089; N=10) that was not significantly correlated with the length of the birds or with their body mass (r<0.24, P>0.5, N=10 for both cases). Thus, the observed variation in swimming speeds among birds was a consequence of the birds' drag coefficients during the glide.

The average $C_{d,glide}$ reported here is intermediate between the values calculated for a model and for carcasses of the Brandt's cormorant (*P. pencillatus*) towed in a water tunnel by Lovvorn et al. (2001). Our value for $C_{d,glide}$ at Re=1.12×10^6 using surface area as a reference (see Table 1 for the conversion factor) was 0.0186±0.0014. This value is higher than that reported for a featherless model, but slightly lower than the value reported for a frozen carcass (~0.008 and ~0.022, respectively, at Re=10^6; data taken from figs 6 and 7 in Lovvorn et al., 2001). Drag measurements on carcasses of birds tend to overestimate the drag coefficient due to feather fluttering (Pennycuick et al., 1988; Tucker, 1990). The featherless model, on the other hand, underestimates the true drag of the birds during the glide by measuring drag at zero lift (θ=0).

Our original application of the burst-and-glide model was to calculate drag coefficients and drag for the entire paddling cycle of the cormorants. However, the model also provides a tool with which to explore the energetic benefit (if existing) of the paddling cycle of these birds. The values of R_p and R that were calculated in our case are rather hypothetical because the burst-and-glide model was designed for animals such as fish that can develop constant thrust. In the original model, the energy required for a fish to overcome water resistance during swimming is compared between swimming at constant speed and swimming at periodically varying speeds oscillating around the same average swimming speed. The paddling of the cormorant, with both feet moving together, is different from this scenario due to existence of the recovery stage. Cormorants can never truly swim at constant speed since the body decelerates during the recovery stage. Therefore, the R and R_p we obtained from the model is the energetic saving from the burst-and-glide swimming pattern relative to the energy required for swimming at constant speed, which is only theoretical. Another difference is the fact that although the recovery is a continuation of the glide (since the body continues to decelerate), it is also part of the burst stage, since without it there is no constant paddling. To deal with these special characteristics of paddling we included the recovery stage in the burst, and therefore compared the energetic saving from combining glides with propulsion, as opposed to paddling constantly at the same average speed.

The values we found for R_p (Table 3, Fig. 6A) suggested that most of our birds were gaining little from combining glides with the paddling cycle. As the average swimming speed became increasingly lower than U_e, the energetic advantage from burst-and-glide diminished to a point where, according to the model, the birds that would propel constantly would save more energy than the birds that added glides to their paddling cycle (R_p>1). The inverse relation between swimming speed and R_p is predicted by the burst-and-glide model. Weihs (1974) has shown that for a given α, R increases (energy saving decreases) when the average swimming speed is reduced with respect to U_e. Therefore, for each value of α there is a minimum average swimming speed where burst-and-glide becomes inefficient. Swimming below this threshold speed will result in R>1. In addition to this the threshold speed decreases as α becomes higher. This way, birds with a higher α benefit from burst-and-glide even at slower swimming speeds. The slower birds in our experiments had the lowest values of α due to the fact that their $C_{d,glide}$ was relatively higher. This elevated $C_{d,glide}$ was due to the need to counter buoyancy at shallow depths. It follows that at deeper depths, where buoyancy of the birds is reduced, $C_{d,glide}$ will

decrease (due to a decrease in the angle-of-attack). $C_{d,stroke}$ does not seem to be related to buoyancy as $C_{d,glide}$, and if this is indeed the case then α should increase with depth, making burst-and-glide more beneficial. This conjecture can be validated by Eqn 7 and 14 above. If we assume that birds swim with the same U_i and U_f but at deeper depth so that their buoyancy is reduced, and also $C_{d,glide}$, then the birds deceleration during the glide stage should reduce as well. Since U_i and U_f remain the same, the birds glide for longer to decelerate from U_f to U_i (or from U_f to U_r), thereby traversing a larger distance of L_g. Since L_g is the numerator in Eqn 7 and 14, the larger L_g for the same set of U_i and U_f results in a larger α. Therefore, the ineffective burst-and-glide observed here ($R_p \geqslant 1$) may prove beneficial at larger depths where buoyancy of the birds is lower.

Fig. 6 shows that the transition from benefit to loss (R_p=1) from adding glides to the paddling cycle occurs at an average swimming speed of about 1.5 m s^{-1}, which is identical to the mean swimming speed observed in our birds. Therefore, only birds that swim at high speeds may gain from adding a glide to their paddling cycle, relative to constant paddling. Yet, all the birds were adding glides to all paddling cycles, regardless of their average speed. The reason is that R_p is a conservative estimate. As mentioned above, the recovery stage is part of the propulsion, on one hand, but it is also part of the deceleration, on the other. When we add the recovery to the stroke stage, we reduce the average acceleration during the burst stage, lower the average drag coefficient for the burst stage ($C_{d,propulsion}$), lengthen the burst stage, and shorten the deceleration stage. This makes paddling less costly relative to gliding (α becomes smaller) and hence the gain in gliding diminishes. However, during the recovery stage the bird continues to move forward (L_r) at a lower drag coefficient and without adding thrust. If the model is rearranged, with the recovery stage added to the glide stage, then the burst stage shortens, it has a higher drag coefficient and the deceleration stage is longer. The R calculated this way (Eqn 7–13) is mostly below 1, and the threshold swimming speed shifts to ~1.0 m s^{-1} (Fig. 6). This speed is similar to the minimal average swimming speed observed from our birds (1.154 m s^{-1}; bird 8). The true energetic benefit and threshold swimming speed are somewhere in between these extreme values for R and U.

The R and R_p values express the energy savings from using burst-and-glide *vs* swimming at constant speed. A hypothetical scenario where cormorants are able to swim at constant speed is one where the birds will use alternate paddling underwater. Cormorants only use alternate paddling while swimming on the surface and use synchronized strokes only underwater (Ancel et al., 2000; Lovvorn, 1991). It is thus interesting to note that the transition between alternate paddling and synchronized strokes should occur at a swimming speed of 1.0–1.5 m s^{-1}, which is similar to the findings that surface-swimming Brandt's cormorants switch from surface swimming to submerged swimming at a speeds of about 1.3 m s^{-1} (Ancel et al., 2000). The birds dive primarily to avoid the higher work against drag at the surface, but the point of transit from surface swimming to submerged swimming also encompasses a change in gait, from alternate paddling to synchronized strokes, and this point of transit fits well with the energy saving threshold found in the present study. However, further research is needed to test the suggestion that in paddlers the shift from alternate to synchronized paddling occurs in agreement with burst-and-glide predictions. If the cormorant has indeed a higher α when swimming at the same swimming speed but at deeper depths, then the associated shift of the threshold swimming speed to slower speeds (as predicted by the burst-and-glide model; Weihs, 1974; Fig. 6A) will ensure that burst-and-glide will have a higher benefit with depth making alternate paddling underwater inefficient in practical swimming speeds. The closely related anhinga, however, is similar to the cormorant in shape but has a different foraging strategy. Due to unusual plumage wettability it relies on hydrostatic mechanisms to become neutrally buoyant underwater (Johansgard, 1993). This allows it to swim very slowly underwater and stalk pray (unlike the active pray chasing in the cormorant). Alternate paddling underwater as well as synchronized strokes have been reported for anhingas (Owre, 1967), and this raises the question whether this behavior is associated with burst-and-glide efficiency, as discussed above. If the bird is neutrally buoyant its α should remain constant with depth and so should the trade-off speed. Therefore during slow swimming, anhingas may profit from shifting to alternate paddling when burst-and-glide is no longer effective. Unfortunately this suggestion cannot be evaluated at present due to lack of observations on the relationship between paddling gait and horizontal swimming speed at various depths in anhingas and cormorants.

List of symbols

a	acceleration
A	area (general)
α	ratio between the C_d for active swimming and C_d for gliding
A_w	surface area
C	average linear slope of the inverse instantaneous swimming speed *vs* time
c	components of drag that are not speed dependant ($0.5\rho AC_d$)
C_a	added mass coefficient (general)
$C_{a(\theta)}$	added mass coefficient when the body is tilted at an angle of attack=θ
C_{ax}	added mass coefficient for motion parallel to the length of a body
C_{ay}	added mass coefficient for motion perpendicular (vertical) to the length of a body
C_d	drag coefficient (general)
$C_{d,glide+recovery}$	average drag coefficient during the glide + recovery stage

$C_{d,glide}$	drag coefficient during the glide stage
$C_{d,propulsion}$	average drag coefficient during the power + recovery stage
$C_{d,recovery}$	drag coefficient during the recovery stage
$C_{d,stroke}$	drag coefficient during the power (acceleration) stage
D	hydrodynamic drag force
ρ	density of water (10^3 kg m^{-3})
F	force (general)
l	body length
L_1	distance traversed during the burst in the original burst-and-glide model
L_2	distance traversed during the glide in the original burst-and-glide model
L_g	distance traversed during the glide stage
L_p	distance traversed during the power (acceleration) stage
L_r	distance traversed during the recovery stage
M	mass
m	virtual mass (mass of the body + added mass of water)
R	relative energetic saving from burst-and-glide (in the case of the cormorant: when the recovery stage is considered as part of the glide)
Re	Reynolds number
R_p	relative energetic saving from burst-and-glide when the recovery stage is considered as part of the burst
t_g	duration of the glide stage
t_p	duration of the power stage
t_r	duration of the recovery stage
θ	angle-of-attack
U	speed (general)
$\overline{U}_c$	average swimming speed in the burst-and-glide model divided by U_e
U_c	average swimming speed in the burst-and-glide model
U_e	maximum achievable swimming speed
$\overline{U}_f$	instantaneous speed at the end of the burst stage divided by U
U_f	instantaneous speed at the end of the burst stage
$\overline{U}_i$	instantaneous speed at the start of the burst stage divided by U_e
U_i	instantaneous speed at the start of the burst stage
$\overline{U}_r$	instantaneous speed at the start of the recovery stage divided by U_e
U_r	instantaneous speed at the start of the recovery stage
V	volume
$V^{2/3}$	volume of the bird to the 2/3 power (representing area)
y	half the body height measurement at a point along the body's length
υ	kinematic viscosity of fresh water (at 20°C=~10^{-6} m^2 s^{-1})
z	half the body width measurement at a point along the body's length

Appendix

The 'burst-and-glide' model summarized in brief from Weihs (1974)

Burst-and-glide is an energy saving locomotion strategy where, instead of swimming at a constant speed, an animal accelerates from an initial velocity U_i to a final velocity U_f during a short stage termed 'burst'. It then glides passively (without producing thrust), decelerating until it reaches the initial velocity U_i (glide stage). During this cycle the animal travels at an average swimming speed U_c. To evaluate when burst-and-glide is energetically efficient, the energy expended from this swimming strategy is compared to the energy expended during swimming at constant speed U_c. This is done by calculating the energy ratio R, which is the ratio between the energy needed to burst-and-glide *vs* the energy needed to swim constantly, where in both cases the average swimming speed is U_c. Weihs (1974) showed that R can be calculated from U_i and U_f,(which are obtained directly from observations) if two additional parameters, U_e and α, are known. U_e is the maximum sustained velocity achievable during maximum thrust. It is used to normalize all speeds to a value $\leqslant 1$. The parameter α is the factor describing the increment in drag when an animal perform swimming motions as oppose to gliding passively (rigid body). In his analysis, Weihs (1974) developed equations for the distances traversed (L_1 and L_2) and the time period (t_1 and t_2) during the burst and the glide stages, respectively, and for U_c. In final form these equations are listed below.

The distance traveled during the burst stage (eqn 21 in Weihs, 1974):

$$L_1 = \frac{m}{\alpha c} \ln\left[\cosh B + \left(\frac{U_i}{U_e}\right)\sinh B\right] . \quad \text{(A1)}$$

The distance traveled during the glide stage (eqn 24a in Weihs, 1974):

$$L_2 = \left(\frac{m}{c}\right) \ln\left(\frac{U_f}{U_i}\right) . \quad \text{(A2)}$$

The duration of the burst stage (eqn 22 in Weihs, 1974):

$$t_1 = \frac{1}{\left(\frac{\alpha c U_e}{m}\right)} \tanh^{-1} \frac{\left(\frac{U_f}{U_e} - \frac{U_i}{U_e}\right)}{\left(1 - \frac{U_f U_i}{U_e^2}\right)} . \quad \text{(A3)}$$

The duration of the glide stage (eqn 24b in Weihs, 1974)

$$t_2 = \frac{m}{cU_e}\left(\frac{U_e}{U_i} - \frac{U_e}{U_f}\right). \quad \text{(A4)}$$

The average swimming speed (eqn 25 in Weihs, 1974)

$$U_c = U_e \frac{\alpha \ln\left(\frac{U_f}{U_i}\right) + \ln\left[\cosh B + \left(\frac{U_i}{U_e}\right)\sinh B\right]}{B + \alpha\left(\frac{U_e}{U_i} - \frac{U_e}{U_f}\right)}$$

and

$$B = \tanh^{-1}\frac{\left(\frac{U_f}{U_e} - \frac{U_i}{U_e}\right)}{\left(1 - \frac{U_i U_f}{U_e^2}\right)}. \quad \text{(A5)}$$

m is the virtual mass (mass + added mass of water accelerated with the body) and c is the component of drag that is not dependant on speed (from the drag term $D=0.5\rho A C_d U^2 = cU^2 \rightarrow c = 0.5\rho A C_d$). Both are unknown but will not be required for the final calculation of R, as explained below.

The energy ratio R is (eqn 18 in Weihs, 1974):

$$R = U_e^2 \frac{t_1(t_1+t_2)}{(L_1+L_2)^2}, \quad \text{(A6)}$$

which can be rearranged using Eqn A3, A4 to be an expression including only velocities and distances (see Videler and Weihs, 1982).

$$R = \frac{1}{\left(\frac{U_c}{U_e}\right)^2\left(1 + \frac{L_2}{L_1}\right)} \quad \text{(A7)}$$

(eqn 15 in Videler and Weihs, 1982).

This solution has an advantage in the calculation since using the ratio L_2/L_1 both m and c cancel out and the final equation can be calculated using only U_i, U_f, U_e and α. Thus:

$$\frac{L_2}{L_1} = \frac{(m/c)\ln(U_f/U_i)}{(m/\alpha c)\ln[\cosh B + (U_i/U_e)\sinh B]} = \frac{\alpha \ln(U_f/U_i)}{\ln[\cosh B + (U_i/U_e)\sinh B]}. \quad \text{(A8)}$$

R is the ratio between the energy required for burst-and-glide and the energy required for constant swimming at U_c. For values of $R<1$, burst-and-glide saves energy relative to constant swimming and when $R>1$, constant swimming is more energetically efficient.

This research was funded by the Israeli Ministry of Science and Technology under contract no. 3920. We are grateful for the assistance of Ohad Agranat, Ruth Almon, Shani Set and Shoshana Goldenberg in the experiments. Comments from two anonymous reviewers greatly improved this manuscript. The Video Department of the Technion provided technical support.

References

Alexander, R. M. (1968). *Animal Mechanics*. Seattle: University of Washington Press.

Ancel, A., Starke, L. N., Ponganis, P. J., Van Dam, R. and Kooyman, G. L. (2000). Energetics of surface swimming in Brandt's cormorants (*Phalacrocorax pencillatus brandt*). *J. Exp. Biol.* **203**, 3727-3731.

Bilo, D. and Nachtigall, W. (1980). A simple method to determine drag coefficients in aquatic animals. *J. Exp. Biol.* **87**, 357-359.

Clark, B. D. and Bemis, W. (1979). Kinematics of swimming of penguins at the Detroit Zoo. *J. Zool. Lond.* **188**, 411-428.

Denny, M. W. (1993). *Air and Water*. New Jersey: Princeton University Press.

Fish, F. E. (1984). Mechanics, power output and efficiency of the swimming muskrat (*Ondatra zibethicus*). *J. Exp. Biol.* **110**, 183-201.

Fish, F. E. (1993). Power output and propulsive efficiency of swimming bottlenose dolphins (*Tursiops truncatus*). *J. Exp. Biol.* **185**, 179-193.

Grémillet, D., Wilson, R. P., Storch, S. and Gary, Y. (1999). Three-dimensional space utilization by a marine predator. *Mar. Ecol. Prog. Ser.* **183**, 263-273.

Haury, L. and Weihs, D. (1976). Energetically efficient swimming behavior of negatively buoyant zooplankton. *Limnol. Oceanogr.* **21**, 797-803.

Hedenstrom, A. and Liechti, F. (2001). Field estimates of body drag coefficient on the basis of dives in passerine birds. *J. Exp. Biol.* **204**, 1167-1175.

Hertel, H. (1966). *Structure Form and Movement*. New York: Reinhold.

Hildebrand, F. B. (1956). *Introduction to Numerical Analysis*. New York: McGraw-Hill.

Hoerner, S. F. (1965). *Fluid-Dynamic Drag*. Great Britain: Hoerner Fluid Dynamics.

Hoerner, S. F. (1975). *Fluid-Dynamic Lift*. Great Britain: Hoerner Fluid Dynamics.

Hove, J. R., O'Bryan, L. M., Gordon, M. S., Webb, P. W. and Weihs, D. (2001). Boxfishes (Teleostei: Ostraciidae) as a model system for fishes swimming with many fins: kinematics. *J. Exp. Biol.* **204**, 1459-1471.

Hui, C. A. (1988). Penguin swimming. I. Hydrodynamics. *Physiol. Zool.* **61**, 333-343.

Johansgard, P. A. (1993). *Cormorants, Darters and Pelicans of the World*. Washington: Smithsonian Institute Press.

Lamb, H. (1945). *Hydrodynamics*. New York: Dover Publications.

Lighthill, M. J. (1960). Note on the swimming of slender fish. *J. Fluid Mech.* **9**, 305-317.

Lighthill, M. J. (1970). Aquatic animal propulsion of high hydromechanical efficiency. *J. Fluid Mech.* **44**, 265-301.

Lighthill, M. J. (1971). Large-amplitude elongated-body theory of fish locomotion. *Proc. R. Soc. Lond. B* **179**, 125-138.

Lovvorn, J. R. (1991). Mechanics of underwater swimming in foot propelled diving birds. *Proc. Int. Ornithol. Congr.* **20**, 1868-1874.

Lovvorn, J. R. (2001). Upstroke thrust, drag effects, and stroke-glide cycles in wing-propelled swimming by birds. *Amer. Zool.* **41**, 154-165.

Lovvorn, J. R. and Jones, D. R. (1991). Body mass, volume, and buoyancy of some aquatic birds and their relation to locomotor strategies. *Can. J. Zool.* **96**, 2888-2892.

Lovvorn, J. R., Jones, D. R. and Blake, R. W. (1991). Mechanics of underwater locomotion in diving ducks: drag, buoyancy and acceleration in a size gradient of species. *J. Exp. Biol.* **159**, 89-108.

Lovvorn, J. R., Liggins, G. A., Borstad, M. H., Calisal, S. M. and Mikkelsen, J. (2001). Hydrodynamic drag of diving birds: effects of body size, body shape and feathers at steady speeds. *J. Exp. Biol.* **204**, 1547-1557.

Maybury, W. J. and Rayner, J. M. V. (2001). The avian tail reduces body parasite drag by controling flow separation and vortex shadding. *Proc. R. Soc. Lond. B* **268**, 1405-1410.

Miller, P. J. O., Johnson, M. P., Tyack, P. L. and Terray, E. A. (2004). Swimming gaits, Passive drag and buoyancy of diving sperm whales *Physeter macarocephalus*. *J. Exp. Biol.* **207**, 1953-1967.

Owre, O. T. (1967). Adaptation for locomotion and feeding in the anhinga and the double-crested cormorant. *Ornithol. Monogr.* **6**, 1-138.
Pennycuick, C. J., Obrecht, H. H. and Fuller, M. R. (1988). Empirical estimates of body drag of large waterfowl and raptors. *J. Exp. Biol.* **135**, 253-264.
Prange, H. D. and Schmidt-Nielsen, K. (1970). The metabolic cost of swimming in ducks. *J. Exp. Biol.* **53**, 763-777.
Ribak, G., Weihs, D. and Arad, Z. (2004). How do cormorants counter buoyancy during submerged swimming? *J. Exp. Biol.* **207**, 2101-2114.
Ribak, G., Weihs, D. and Arad, Z. (2005). Water retention in the plumage of diving great cormorants *Phalacrocorax carbo sinensis*. *J. Avian Biol.* **36**, 89-95.
Sato, K., Mitani, Y., Cameron, M. F., Siniff, D. B. and Naito, Y. (2003). Factors affecting stroking patterns and body angle in diving Weddell seals under natural conditions. *J. Exp. Biol.* **206**, 1461-1470.
Schmid, D., Gremillet, D. J. H. and Culik, B. M. (1995). Energetics of underwater swimming in the great cormorant (*Phalacrocorax carbo sinensis*). *Mar. Biol.* **123**, 875-881.
Schultz, W. W. and Webb, P. W. (2002). Power requirements of swimming: do new methods resolve old questions? *Int. Comp. Biol.* **42**, 1018-1025.
Skrovan, R., Williams, T., Berry, P., Moore, P. and Davis, R. (1999). The diving physiology of bottlenose dolphins (*Tursiops truncatus*). II. Biomechanics and changes in buoyancy at depth. *J. Exp. Biol.* **202**, 2749-2761.
Spanier, E., Weihs, D. and Almog-Shtayer, G. (1991). Swimming of the Mediterranean slipper lobster. *J. Exp. Mar. Biol. Ecol.* **145**, 15-31.
Stelle, L., Blake, R. and Trites, A. (2000). Hydrodynamic drag in Steller sea lions (*Eumetopias jubatus*). *J. Exp. Biol.* **203**, 1915-1923.
Stephenson, R. (1994). Diving energetics in lesser scaup (*Aythyta affinis* Eyton). *J. Exp. Biol.* **190**, 155-178.
Thomas, A. L. R. (1996). Why do birds have tails? the tail as a drag reducing flap, and trim control. *J. Theor. Biol.* **183**, 247-253.
Tucker, V. A. (1990). Body drag, feather drag and interference drag of the mounting strut in a peregrine falcon, *Falco peregrinus*. *J. Exp. Biol.* **149**, 449-468.
Van Dam, R. P., Ponganis, P. J., Ponganis, K. V., Levenson, D. H. and Marshall, G. (2002). Stroke frequencies of emperor penguins diving under sea ice. *J. Exp. Biol.* **205**, 3769-3774.
Videler, J. J. and Weihs, D. (1982). Energetic advantages of burst-and-coast swimming of fish at high speeds. *J. Exp. Biol.* **97**, 169-178.
Vogel, S. (1994). *Life in Moving Fluids.* Princeton: Princeton University Press.
Webb, P. W. (1971). The swimming energetics of trout. I. *J. Exp. Biol.* **55**, 489-520.
Webb, P. W. and Fairchild, A. G. (2001). Performance and maneuverability of three species of teleostean fishes. *Can. J. Zool.* **79**, 1866-1877.
Weihs, D. (1974). Energetic advantages of burst swimming of fish. *J. Theor. Biol.* **48**, 215-229.
Weihs, D. (2002). Dynamics of dolphin porpoising revisited. *Integ. Comp. Biol.* **42**, 1071-1078.
Weihs, D. (2004). The hydrodynamics of dolphin drafting. *J. Biol.* **3**, 8.
Williams, T. M. and Kooyman, G. L. (1985). Swimming performance and hydrodynamic characteristics of harbor seals, *Phoca vitulina*. *Physiol. Zool.* **58**, 576-589.
Wilson, R. P., Hustler, K., Ryan, P. G., Burger, A. E. and Noldeke, E. C. (1992). Diving birds in cold water: do Archimedes and Boyle determine energetic costs? *Am. Nat.* **140**, 179-200.